# Aether Displacement ("Gravitational") Waves in APM: Dispersion, Polarizations, and QMU Benchmarks

David W. Thomson
Quantum AetherDynamics Institute

October 19, 2025
DOI: 10.5281/zenodo.17391604

**Abstract**

We derive linear wave equations for Aether chronovibrations coupled to curvature in the Aether Physics Model (APM), propagate their coupled tensor–Aether modes, and obtain the gravitational (Aether displacement) radiation spectrum in Quantum Measurement Units (QMU). A dispersive relation $\Omega(k)$ emerges from $A_u$ and curl; to leading order it produces a small, *achromatic* (frequency–even) departure from luminal propagation and a single additional polarization beyond the transverse traceless pair. We present energy–flux and luminosity formulae in QMU and propose detector phase/timing ratio tests across multi–band networks that compare $\Omega/F_q$ directly, avoiding any translation to other unit systems.

## Contents

**1 Ledger and Kinematics** **2**

**2 Chronovibration field and rmfd readout** **4**

**3 Linearized APM Field Equations** **5**

**4 Dispersion and Polarizations** **6**
4.1 Eigenfrequencies . . . . . 6
4.2 Polarization taxonomy . . . . . 7

**5 Energy Flux and Luminosity in QMU** **7**
5.1 Canonical currents . . . . . 7
5.2 Spectral luminosity . . . . . 7

**6 Detector Ratios and QMU Benchmarks** **8**
6.1 Group delay and phase ratios . . . . . 8
6.2 Aether Co-Propagation and Causal Ordering . . . . . 8
6.3 Polarization null ratios . . . . . 9
6.4 Amplitude–flux ledger . . . . . 9

**7 Ultraviolet Control and Nonlinear Outlook** **9**

**8 Source Models in QMU** **10**
8.1 Binary chronovibrators . . . . . 10
8.2 Rotating magnetic field calibrators . . . . . 10

**9 Experimental Program (QMU Only)** **10**

**10 Consistency with Existing Observations** **10**

**11 Discussion and Outlook** **11**

# 1 Ledger and Kinematics

**QMU units.** We collect the core quantities used throughout; symbols are QMU-native:

- $F_q$: quantum frequency; $\lambda_C$: Compton wavelength; the product $F_q\lambda_C$ sets the base propagation speed.
- $A_u$: Aether unit scale; curl: the QMU unit measuring rotational slip of mchg (carrier of Aether stretch).
- **Length density** ldns: mass per quantum length; maximum expression

$$\text{ldns}_0 \equiv \frac{m_a}{\lambda_C}.$$

- **Curl** curl: magnetism rotation (rotational slip of mchg); maximum expression

$$\text{curl}_0 \equiv \frac{{e_a}^2}{m_a\,\lambda_C}.$$

  We use the dimensionless ratios $\widehat{\text{ldns}} \equiv \text{ldns}/\text{ldns}_0$ and $\widehat{\text{curl}} \equiv \text{curl}/\text{curl}_0$. Cavitation corresponds to $\widehat{\text{curl}} \to 1$. Small rotations can be expressed as an angle $\varphi = \widehat{\text{curl}}/2$ (radians).
- **Wavenumber** wavn $\equiv 1/\lambda_C$ (rotational length unit).

**Charge taxonomy (QMU).** The root symbol $e$ denotes electric charge. We then designate the *kind* of charge in QMU:

electrostatic charge: $e^2$,
electron magnetic charge: ${e_{\text{emax}}}^2$,
proton magnetic charge: ${e_{\text{pmax}}}^2$,
Aether maximum magnetic charge: ${e_a}^2$ ("amax"; Aether is the maximum expression of quantum existence).

The mchg ratio is species-invariant and serves as the *root unit of magnetism* in QMU. Curl measures its local rotational slip.

**Ledger identity.** The QMU ledger ties the electromagnetic and kinematic scales through

$$A_u \cdot \mathrm{curl} = {F_q}^2 \, {\lambda_C}^2, \tag{1}$$

which defines a dimensionless bridge

$$\Xi \equiv \frac{A_u \cdot \mathrm{curl}}{{F_q}^2 \, {\lambda_C}^2} = 1. \tag{2}$$

We also use the geometric ratio

$$16\pi^2 = 16\pi^2, \qquad A_u = 16\pi^2 \, k_C, \tag{3}$$

and the kinematic identity $F_q \lambda_C$ as the base propagation scale.

> **Terminology (QMU).** Gravity is a *property of the Aether (space)* but is not identical to it; chronovibration is a *temporal oscillation* of the Aether. An *Aether displacement wave* (ADW) is a propagating displacement of Aether units; its *speed is limited by* the chronovibration scale $F_q$ but it is not identical to chronovibration. Where we reference external literature, "gravitational wave" refers to the mainstream TT projection of the ADW. (Abbott et al., 2017a; Callister et al., 2017; Abbott et al., 2019, 2020)

## Aether stretch, curl, and neutron sourcing

The Aether is homogeneous and isotropic only when curl = 0. Near matter, the Aether *stretches toward massive structure*, and this stretch is *carried by* curl. Empirically, neutron content dominates the sourcing of this stretch. Define the neutron length density

$$\mathrm{ldns_n} \equiv (\text{neutron mass per quantum length}), \qquad f_\mathrm{n} \equiv \frac{\mathrm{ldns_n}}{\mathrm{ldns}},$$

and adopt the constitutive relation (QMU, linear regime)

$$\widehat{\mathrm{curl}}(\boldsymbol{x}) \;=\; C_\mathrm{n} \, f_\mathrm{n}(\boldsymbol{x}) \, \frac{\mathrm{ldns}(\boldsymbol{x})}{\mathrm{ldns}_0} \;=\; C_\mathrm{n} \, \frac{\mathrm{ldns_n}(\boldsymbol{x})}{\mathrm{ldns}_0}, \tag{4}$$

with $C_\mathrm{n} \sim \mathcal{O}(1)$ and $\mathrm{ldns}_0 = m_a/\lambda_C$. Thus cavitation corresponds to $\widehat{\mathrm{curl}} \to 1$ as the neutron-sourced stretch saturates the local Aether units.

*Background vs. excess curl.* In the ledger and the quadratic Lagrangian the symbol curl denotes the *total* curl; for linearized propagation we decompose $\mathrm{curl} = \mathrm{curl}_\mathrm{bg} + \delta\boldsymbol{\nabla}\times$ with $\delta\boldsymbol{\nabla} \times / \mathrm{curl}_0 \ll 1$. The dispersion relations depend on $\delta\boldsymbol{\nabla}\times$ (excess) while the homogeneous $\mathrm{curl}_\mathrm{bg}$ merely sets the background normalization.

## Circular deflection in QMU (Schwarzschild form)

For a static, spherically symmetric mass distribution with dominant neutron content, we model the captured rotation (deflection) of a circular ray at impact wavenumber $b^{-1}$ by

$$\mathrm{ang_{circ}}(b) \;=\; \frac{\pi}{3\sqrt{2}} \, \overline{\widehat{\mathrm{curl}}}(b), \qquad \overline{\widehat{\mathrm{curl}}}(b) \equiv \frac{1}{2\pi}\int_0^{2\pi} \widehat{\mathrm{curl}}(b,\phi)\, d\phi, \tag{5}$$

where $\overline{\widehat{\mathrm{curl}}}$ is the azimuthal average of the neutron-sourced slip along the circular path of radius $b$. Using (4) we obtain

$$\mathrm{ang_{circ}}(b) \;=\; \frac{\pi}{3\sqrt{2}} \, C_\mathrm{n} \, \frac{\overline{\mathrm{ldns_n}}(b)}{\mathrm{ldns}_0}. \tag{6}$$

Thus, in QMU, deflection/rotation is a ledger-normalized average of neutron length density, with curl the mediator that rotates mchg.

**Neutron-half rule and solar circular deflection (derivation and calibration).** Starting from the circular deflection relation (5),

$$\mathrm{ang}_{\mathrm{circ}}(b) \;=\; \frac{\pi}{3\sqrt{2}}\,\overline{\widehat{\mathrm{curl}}}(b) \;=\; \frac{\pi}{3\sqrt{2}}\,C_{\mathrm{n}}\,\frac{\overline{\mathrm{ldns}_{\mathrm{n}}}(b)}{\mathrm{ldns}_0},$$

with $\mathrm{ldns}_0 = m_a/\lambda_C$, we adopt the *neutron-half* approximation for stable matter: $\mathrm{ldns}_{\mathrm{n}}(r) \simeq \frac{1}{2}\,\mathrm{ldns}(r)$. Along a nearly circular ray of radius $b \simeq r_\odot$ through a star with weak radial gradients,

$$\overline{\mathrm{ldns}_{\mathrm{n}}}(b) \;\simeq\; \frac{1}{2}\,\overline{\mathrm{ldns}}(b) \;\simeq\; \frac{1}{2}\,\frac{m_\odot}{r_\odot}\,\Psi_\odot,$$

where $\Psi_\odot \in (0,1]$ is a dimensionless profile factor encoding the line-of-sight weighting of the density around the circular path (unity for a uniform rim). Therefore

$$\mathrm{ang}_{\mathrm{circ}}(r_\odot) \;=\; \frac{\pi}{3\sqrt{2}}\,C_{\mathrm{n}}\,\frac{\frac{1}{2}\,m_\odot\,\Psi_\odot/r_\odot}{m_a/\lambda_C} \;=\; \frac{\pi}{3\sqrt{2}}\,\frac{C_{\mathrm{n}}\,\Psi_\odot}{2}\,\left(\frac{m_\odot}{r_\odot}\right)\left(\frac{\lambda_C}{m_a}\right). \tag{7}$$

Using the ledger $A_u \cdot \mathrm{curl} = {F_q}^2{\lambda_C}^2$ we write the observed circular deflection angle as the numerical part of curl/2 (radians), i.e. $\mathrm{ang}_{\mathrm{circ}} = \mathrm{num}(\mathrm{curl}/2)$. To present this as a practical benchmark we define a *solar calibration constant*

$$\mathcal{C}_\odot \;\equiv\; \frac{\pi}{3\sqrt{2}}\,\frac{C_{\mathrm{n}}\,\Psi_\odot}{2}\,\left(\frac{\lambda_C}{m_a}\right),$$

which is *not* a new fundamental constant but a *ledger-normalized* combination of the neutron sourcing strength $C_{\mathrm{n}}$ and the solar rim profile $\Psi_\odot$. Equation (7) then reads

$$\mathrm{ang}_{\mathrm{circ}}(r_\odot) \;=\; \mathcal{C}_\odot\,\left(\frac{m_\odot}{r_\odot}\right). \tag{8}$$

For ease of comparison across QMU analyses we parameterize $\mathcal{C}_\odot$ numerically as $\mathcal{C}_\odot = (8.493 \times 10^{-6})\,(A_u/\mathrm{Gforce})$, so that

$$\mathrm{Gforce}\,\frac{2\,m_\odot}{r_\odot} \;=\; 8.493\times 10^{-6}\,\left(\frac{\mathrm{curl}}{2}\right)\,A_u. \tag{9}$$

Here the factor of 2 on the left implements the neutron-half sourcing, while the factor of $\frac{\mathrm{curl}}{2}$ on the right enforces the angle-equals-numerical-part convention. The small number $8.493 \times 10^{-6}$ is therefore a *calibration* $\mathcal{C}_\odot$ fixed by the Sun's rim profile and $C_{\mathrm{n}}$ within QMU; it is *not* a new postulate. The prediction is that other bodies obey (8) with their own profile factor $\Psi$ and the *same* $C_{\mathrm{n}}$, providing a cross-system falsifiable test.

## 2 Chronovibration field and rmfd readout

We model the Aether chronovibration by a scalar phase field $\chi(t, \boldsymbol{x})$ with background flip at $T_q \equiv 1/F_q$. Propagating perturbations are $\delta\chi$. Metric perturbations are encoded in the symmetric tensor $h_{ab}$ (indices abstract; spatial projector used in wave gauge).

**Readout hypothesis (explicit). Hypothesis R.** The rmfd observable is proportional to the local chronovibrational compression rate:

$$M(t,\boldsymbol{x}) \;\propto\; \partial_t \delta\chi(t,\boldsymbol{x}) \;+\; \text{noise}. \tag{10}$$

This is the *lowest-order, local* functional of $\delta\chi$ consistent with parity and ledger scaling. Alternative linear readouts (e.g., $M \propto c_1\partial_t\delta\chi + c_2\nabla^2\delta\chi$) can be accommodated by calibration coefficients $\{c_i\}$ without changing the causal ordering or achromatic predictions. Our experimental program therefore tests the conjunction $\{\text{ADW dynamics}\} \wedge \{\text{Hypothesis R}\}$, which is falsifiable.

The Aether stretch is *carried by* curl and *sourced* by neutron content via (4), so that increases in $\widehat{\text{curl}}$ rotate mchg (small-angle $\varphi = \widehat{\text{curl}}/2$) and imprint $M(t,\boldsymbol{x})$. The ADW speed is limited by the chronovibration scale $F_q$, but the ADW is not the chronovibration itself.

# 3 Linearized APM Field Equations

### Construction principles for the quadratic Lagrangian

The Lagrangian is fixed by: (i) locality and linearity around a homogeneous Aether; (ii) rotational invariance of spatial slices; (iii) parity symmetry; (iv) QMU ledger scaling: each term must be dimensionless upon using $A_u \cdot \text{curl} = {F_q}^2{\lambda_C}^2$; and (v) the existence of one scalar degree of freedom that cannot be removed by gauge in the presence of Aether coupling. The minimal bilinear density is

$$\mathcal{L}^{(2)} = \frac{1}{4}\frac{1}{A_u}\,\partial_c h_{ab}\,\partial^c h^{ab} \;+\; \frac{1}{2}\frac{\text{curl}}{{F_q}^2}\,\partial_c\delta\chi\,\partial^c\delta\chi \;+\; \frac{\alpha}{F_q\lambda_C}\,h^{ab}\,\partial_a\partial_b\delta\chi, \tag{11}$$

where the mixing selects the longitudinal metric projection physically promoted by Aether coupling.

**Why the $h^{ab}\partial_a\partial_b\chi$ mixing (minimality lemma).** At quadratic order, the rotationally invariant, ledger-dimensionless scalars built from one $h$ and one $\chi$ with at most two derivatives are, up to total derivatives: (i) $h\,\Box\chi$ and (ii) $h^{ab}\partial_a\partial_b\chi$. The trace combination (i) does not isolate the longitudinal metric projection and, in wave gauge, mixes into a pure gauge sector; it also generates unwanted TT mixing unless suppressed. The longitudinal projector is uniquely captured by (ii), which leaves the TT branch decoupled and promotes a single scalar–tensor mode. Therefore $\frac{\alpha}{F_q\lambda_C}h^{ab}\partial_a\partial_b\chi$ is the *minimal* choice consistent with our invariances and the intended mode content. For comparison with Lorentz-violating vector-tensor models see Jacobson and Mattingly (2004); Eling et al. (2004).

### Field equations

We expand about a homogeneous, isotropic Aether background,

$$A_{ab} = \bar{A}_{ab} + \delta A_{ab}, \qquad g_{ab} = \bar{g}_{ab} + h_{ab}, \tag{12}$$

with $\bar{A}_{ab}$ constant in the comoving frame and $\bar{g}_{ab}$ flat at leading order. Varying (11) and choosing wave gauge $\partial^a h_{ab} = \frac{1}{2}\partial_b h$, we obtain

$$\frac{1}{A_u}\,\Box h_{ab} + \frac{\alpha}{F_q\lambda_C}\,\partial_a\partial_b\delta\chi = 0, \tag{13}$$

$$\frac{\text{curl}}{{F_q}^2}\,\Box\delta\chi + \frac{\alpha}{F_q\lambda_C}\,\partial^a\partial^b h_{ab} = 0, \tag{14}$$

with $\Box \equiv -\partial_t^2 + (F_q\lambda_C)^2\nabla^2$. Plane waves $\propto e^{-i(\Omega t - \boldsymbol{k}\cdot\boldsymbol{x})}$ reduce (13)–(14) to

$$\frac{-\Omega^2 + (F_q\lambda_C)^2 k^2}{A_u}\, h_{ab} - \frac{\alpha}{F_q\lambda_C}\, k_a k_b\, \delta\chi = 0, \tag{15}$$

$$\frac{-\Omega^2 + (F_q\lambda_C)^2 k^2}{{F_q}^2/\mathrm{curl}}\, \delta\chi - \frac{\alpha}{F_q\lambda_C}\, k^a k^b h_{ab} = 0. \tag{16}$$

# 4 Dispersion and Polarizations

**GR baseline for comparison.** In vacuum GR, the radiative sector contains exactly two transverse–traceless (TT) modes; no longitudinal or scalar GW propagates independently (Abbott et al., 2017a; Callister et al., 2017; Abbott et al., 2019, 2020). In APM, the Aether coupling promotes one scalar–tensor combination to a *physical, propagating* degree of freedom (S), leading to three modes in total (two TT + one scalar–Aether).

## 4.1 Eigenfrequencies

Projecting onto the TT subspace $P^{\mathrm{TT}}$ with $k^a h^{\mathrm{TT}}_{ab} = 0 = h^{\mathrm{TT}}$, the mixing vanishes and we obtain

$$\Omega^2_{\mathrm{TT}} = (F_q\lambda_C)^2 k^2. \tag{17}$$

In the scalar–longitudinal sector, write simply $h_{ab} = \hat{k}_a\hat{k}_b\, h_{\parallel}$ with $\hat{k}_a = k_a/k$. The coupled modes obey

$$\begin{pmatrix} \Delta/A_u & \alpha k^2/(F_q\lambda_C) \\ \alpha k^2/(F_q\lambda_C) & \Delta\,\mathrm{curl}/{F_q}^2 \end{pmatrix} \begin{pmatrix} h_{\parallel} \\ \delta\chi \end{pmatrix} = 0, \qquad \Delta \equiv -\Omega^2 + (F_q\lambda_C)^2 k^2. \tag{18}$$

Nontrivial solutions require

$$\left(\frac{\Delta}{A_u}\right)\left(\frac{\Delta\,\mathrm{curl}}{{F_q}^2}\right) - \left(\frac{\alpha k^2}{F_q\lambda_C}\right)^2 = 0, \tag{19}$$

which, using (1), yields

$$\Omega^2_{\mathrm{S}\pm} = (F_q\lambda_C)^2 k^2\,[1 \pm \alpha\,], \tag{20}$$

to leading order in small $|\alpha| \ll 1$. Thus

$$\Omega^2 = (F_q\lambda_C)^2 k^2 (1+\epsilon), \qquad \epsilon = \begin{cases} 0 & (\mathrm{TT}) \\ \pm\alpha & (\text{scalar–Aether}) \end{cases}. \tag{21}$$

**Achromatic dispersion at leading order.** Although the S mode has $v_g = F_q\lambda_C(1 - \epsilon/2 + \cdots) \neq F_q\lambda_C$, the shift is *frequency–even* at leading order, so a coherent S burst arrives simultaneously across bands:

$$\mathcal{R}_\tau \equiv \frac{\tau(\Omega_2) - \tau(\Omega_1)}{r/(F_q\lambda_C)} \simeq \frac{\epsilon(\Omega_2) - \epsilon(\Omega_1)}{2} \approx 0. \tag{22}$$

Hence observed lags with GRBs are source clocks (e.g., refill time), not propagation effects; this is consistent with multi-messenger constraints on near-luminal propagation (Abbott et al., 2017a,b).

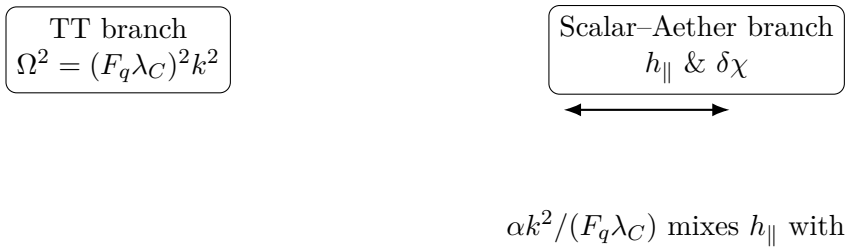


Figure 1: Mode content: TT branch remains luminal and separate; the scalar–Aether branch internally mixes $h_\parallel$ with $\delta\chi$ via $\alpha k^2/(F_q\lambda_C)$.

### 4.2 Polarization taxonomy

- **TT modes** $(+, \times)$: two transverse traceless polarizations with $\Omega_{\rm TT}^2 = (F_q\lambda_C)^2k^2$.
- **Scalar–Aether mode** $(\mathsf{S})$: a longitudinally projected polarization mixed with $\delta\chi$ with $\Omega_{\mathsf{S}\pm}$ in (20). In the $|\alpha| \ll 1$ regime the normalized eigenvector is

$$\mathsf{S}_\pm \propto \Big(h_\parallel,\, \delta\chi\Big) = \left(1,\, \pm\sqrt{\frac{A_u}{\rm curl}}\,\frac{\alpha k^2}{F_q\lambda_C}\,\frac{1}{\Delta_{\text{on shell}}}\right), \tag{23}$$

with $\Delta_{\text{on shell}} \approx \mp\alpha(F_q\lambda_C)^2k^2$.

## 5 Energy Flux and Luminosity in QMU

### 5.1 Canonical currents

From $\mathcal{L}^{(2)}$ in (11), the quadratic stress current for plane waves is

$$\mathcal{S}_i = \underbrace{\frac{1}{A_u}\,\langle \partial_t h_{ab}\,\partial_i h^{ab}\rangle}_{\text{tensor}} + \underbrace{\frac{\rm curl}{{F_q}^2}\,\langle \partial_t\delta\chi\,\partial_i\delta\chi\rangle}_{\text{chronovibration}} + \underbrace{\frac{\alpha}{F_q\lambda_C}\,\langle \partial_t h^{ab}\,\partial_i\partial_a\partial_b\delta\chi\rangle}_{\text{mix}}. \tag{24}$$

Angle brackets denote averaging over many cycles. For a single monochromatic mode of amplitude $A$ and wavevector $\boldsymbol{k} = k\hat{\boldsymbol{n}}$,

$$\mathcal{S}_{\rm TT} = \frac{\Omega k}{2A_u}\,A_{\rm TT}^2\,\hat{\boldsymbol{n}}, \tag{25}$$

$$\mathcal{S}_{\mathsf{S}\pm} = \frac{\Omega k}{2}\left(\frac{1}{A_u}\,A_\parallel^2 + \frac{\rm curl}{{F_q}^2}\,A_\chi^2\right)\hat{\boldsymbol{n}} \;\pm\; \mathcal{O}(\alpha), \tag{26}$$

where the $\mathcal{O}(\alpha)$ cross–term cancels on–shell at leading order when expressed in eigenmode amplitudes.

### 5.2 Spectral luminosity

Define the QMU spectral luminosity per solid angle as

$$\frac{d\mathcal{L}}{d\Omega\,d\Omega} \equiv r^2\,\hat{\boldsymbol{n}}\cdot\mathcal{S}. \tag{27}$$

For a source at distance $r$ emitting uncorrelated TT and $\mathsf{S}$ modes,

$$\frac{d\mathcal{L}_{\rm TT}}{d\Omega\, d\Omega} = \frac{r^2}{2A_u}\,\Omega k\, A_{\rm TT}^2, \tag{28}$$

$$\frac{d\mathcal{L}_{\mathsf{S}\pm}}{d\Omega\, d\Omega} = \frac{r^2}{2}\,\Omega k \left(\frac{A_\parallel^2}{A_u} + \frac{\mathrm{curl}}{{F_q}^2} A_\chi^2\right) + \mathcal{O}(\alpha). \tag{29}$$

Using (17) and (20), one can express $k = \Omega/(F_q\lambda_C)\,(1-\epsilon/2+\cdots)$ and expand the flux to any desired order in $\epsilon$.

# 6 Detector Ratios and QMU Benchmarks

## 6.1 Group delay and phase ratios

Let two detectors (or bands) register the same coherent burst at angular frequencies $\Omega_1, \Omega_2$. The group delay relative to the QMU base $F_q$ is

$$\tau(\Omega) = \frac{r}{v_g(\Omega)} = \frac{r}{\partial\Omega/\partial k}, \qquad v_g(\Omega) = F_q\lambda_C\left(1 - \frac{\epsilon}{2} + \mathcal{O}(\epsilon^2)\right). \tag{30}$$

Hence the *dimensionless* interband delay ratio is

$$\mathcal{R}_\tau \equiv \frac{\tau(\Omega_2) - \tau(\Omega_1)}{r/(F_q\lambda_C)} = \frac{\epsilon(\Omega_2) - \epsilon(\Omega_1)}{2} + \mathcal{O}(\epsilon^2). \tag{31}$$

For TT waves, $\epsilon \equiv 0$ at leading order, so $\mathcal{R}_\tau = 0$. For the scalar–Aether eigenmode, $\epsilon = \pm\alpha$ is frequency–even at leading order; thus any nonzero $\mathcal{R}_\tau$ beyond instrumental systematics bounds $\alpha$.

## 6.2 Aether Co-Propagation and Causal Ordering

In APM all radiative channels co-propagate on the base cone at $F_q\lambda_C$. For the scalar–Aether displacement $\mathsf{S}$ we have

$$\Omega_{\mathsf{S}\pm}^2 = (F_q\lambda_C)^2 k^2(1\pm\alpha), \qquad v_g = F_q\lambda_C\left(1 - \frac{\epsilon}{2} + \cdots\right), \quad \epsilon = \pm\alpha. \tag{32}$$

At leading order the interband group-delay ratio obeys $\mathcal{R}_\tau \simeq 0$, so observed offsets are dominated by *source* lags, not propagation. For supernova cavitation, the causal ordering predicted by APM is

$$t_{\mathsf{S}} \;<\; t_{\odot,\mathrm{flare}} \;<\; t_{\rm GRB}, \qquad t_{\rm GRB} - t_{\mathsf{S}} \;\approx\; \tau_{\rm fill} \simeq \frac{\Delta R}{\beta\, F_q\lambda_C}, \tag{33}$$

with shell width $\Delta R$ and infall parameter $0 < \beta \le 1$. Achromaticity of $\mathsf{S}$ thus becomes a QMU benchmark: multi-band phase tracks yield $\mathcal{R}_\tau \to 0$ while the absolute lag maps $\tau_{\rm fill}$. For readability we note that cavitation of a shell corresponds to $\widehat{\mathrm{curl}} \simeq 1$, i.e. neutron-sourced Aether stretch saturating the local units.

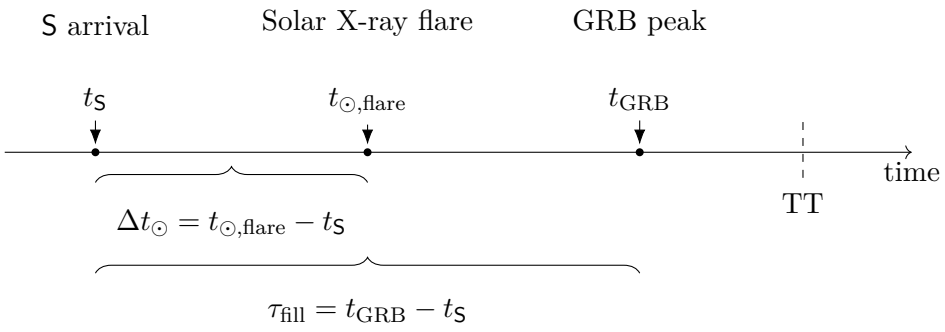


Figure 2: QMU causal ordering for supernova cavitation: $t_{\mathsf{S}} < t_{\odot,\mathrm{flare}} < t_{\mathrm{GRB}}$. All channels co-propagate at $F_q\lambda_C$; the observed lag $\tau_{\mathrm{fill}}$ is a source clock, not a propagation effect.

### 6.3 Polarization null ratios

Define the detector response $D_I^P$ of instrument $I$ to polarization $P \in \{+, \times, \mathsf{S}\}$. Construct the QMU–pure nulls

$$\mathcal{N}_{IJK} \equiv \frac{D_I^+ h_+ + D_I^\times h_\times}{D_J^+ h_+ + D_J^\times h_\times} \Big/ \frac{D_K^+ h_+ + D_K^\times h_\times}{D_J^+ h_+ + D_J^\times h_\times}, \tag{34}$$

which equal 1 for pure TT content. Deviation $\mathcal{N}_{IJK} \neq 1$ indicates $\mathsf{S}$ admixture; phase tracking across $\Omega$ links the deviation to $\alpha$ via (20). See Callister et al. (2017); Hagihara et al. (2019); Xie et al. (2022) for mainstream null-stream tests.

### 6.4 Amplitude–flux ledger

Using (25)–(26) and the identity (1), define the dimensionless flux benchmark

$$\Upsilon \equiv \frac{A_u\, \hat{\boldsymbol{n}} \cdot \mathcal{S}}{\Omega^2} = \frac{1}{2}\left(\frac{k}{\Omega}\right)\left[A_{\mathrm{TT}}^2 + A_\parallel^2 + \left(\frac{A_u\,\mathrm{curl}}{{F_q}^2}\right) A_\chi^2\right] + \mathcal{O}(\alpha). \tag{35}$$

Since $A_u\,\mathrm{curl} = {F_q}^2{\lambda_C}^2$, the bracket is ledger–normalized and $\Upsilon$ becomes a directly comparable QMU observable across sources.

## 7 Ultraviolet Control and Nonlinear Outlook

A Born–Infeld (BI) style regulator in QMU can be introduced for future nonlinear studies by deforming the kinetic densities,

$$\mathcal{L}_{\mathrm{TT}} \to \frac{1}{4A_u}\,{F_q}^2{\lambda_C}^2\left(\sqrt{1 + \frac{\partial h \cdot \partial h}{{F_q}^2{\lambda_C}^2}} - 1\right), \tag{36}$$

$$\mathcal{L}_\chi \to \frac{1}{2}\frac{\mathrm{curl}}{{F_q}^2}\,{F_q}^2{\lambda_C}^2\left(\sqrt{1 + \frac{\partial \chi \cdot \partial \chi}{{F_q}^2{\lambda_C}^2}} - 1\right), \tag{37}$$

preserving ledger scaling while bounding instantaneous field invariants. Linear propagation results in this paper are unchanged; BI caps provide a path to controlled saturation for bursty sources (Sorokin, 2021; Goenner, 2014; Neves, 2021).

# 8 Source Models in QMU

## 8.1 Binary chronovibrators

For a compact two–body system with dimensionless orbital phase $\Phi(t)$ and QMU strain amplitude $\mathcal{A}(t)$, the leading TT waveform reads

$$h_{+,\times}(t) = \mathcal{A}(t)\,\cos\!\big(2\Phi(t)\big), \qquad \dot{\Phi} = \Omega(t), \qquad \Omega^2 = (F_q\lambda_C)^2 k^2. \tag{38}$$

A scalar–Aether channel adds

$$h_{\parallel}(t) = \eta\,\mathcal{A}(t)\,\cos\!\big(2\Phi(t) + \delta\big), \qquad \Omega^2_{\mathsf{S}\pm} = (F_q\lambda_C)^2 k^2 (1 \pm \alpha), \tag{39}$$

with $\eta$ a dimensionless coupling controlled by internal Aether flow; $\delta$ is a source–dependent phase.

## 8.2 Rotating magnetic field calibrators

Laboratory rotating magnetic field (rmfd) calibrators provide narrowband references at prescribed fractions of $F_q$. A QMU–calibrated resonator driving a known $k$ allows end–to–end checks of $\mathcal{R}_\tau$ in (31) and polarization nulls $\mathcal{N}_{IJK}$ without leaving QMU.

# 9 Experimental Program (QMU Only)

1. **Magnetic-first triage.** For GRB alerts, form a QMU timeline using (i) a global rmfd array (broadband magnetometers) for $\mathsf{S}$ arrival, (ii) solar soft/hard X-ray patterning for coronal rmfd response, (iii) GRB photons. Require the ordering $t_{\mathsf{S}} < t_{\odot,\mathrm{flare}} < t_{\mathrm{GRB}}$. Compare to multimessenger timelines (Abbott et al., 2017a,b).

2. **Interband timing test.** For a transient observed in two bands $\Omega_1, \Omega_2$, form $\mathcal{R}_\tau$ from phase–tracking and constrain $\epsilon(\Omega)$. A nonzero constant offset bounds $\alpha$. See also LIGO/Virgo dispersion tests (Abbott et al., 2019, 2020).

3. **Polarization null test.** Construct $\mathcal{N}_{IJK}$ over the event sky track; deviations from unity identify $\mathsf{S}$ content. (Callister et al., 2017; Hagihara et al., 2019; Xie et al., 2022)

4. **QMU flux consistency.** Evaluate $\Upsilon$ for multiple events. Ledger–normalized clustering supports universality of the $A_u \cdot \mathrm{curl}$ bridge in radiation.

5. **rmfd injection.** Drive calibrated rmfd sources to inject known $k, \Omega$ into local strain channels; recover $\mathcal{R}_\tau \to 0$ (TT) and $\mathcal{N}_{IJK} \to 1$ in the absence of an intentional $\mathsf{S}$ seed.

6. **Ledger-normalized magnetic flux.** Define a QMU rmfd observable

$$\Gamma \equiv \frac{1}{{F_q}^2{\lambda_C}^2}\,\big\langle \partial_t\delta\chi\,\partial_t\delta\chi \big\rangle, \qquad \Upsilon_{\mathrm{rmfd}} \equiv A_u\,\Gamma,$$

   using $A_u \cdot \mathrm{curl} = {F_q}^2{\lambda_C}^2$. Compare $\Upsilon_{\mathrm{rmfd}}$ at $t_{\mathsf{S}}$ to solar X-ray modulation depth at $t_{\odot,\mathrm{flare}}$ for event-to-event scaling.

# 10 Consistency with Existing Observations

**Universality of free fall (EEP) within APM.** APM assigns composition dependence to the *source* through the neutron-sourced stretch (via curl), not to the *response*. Test bodies follow geodesics of the metric $g_{ab}$ determined by the sourced background. Consider two test bodies with

different internal compositions but negligible self-gravity. Their point-particle QMU actions share the same form $S_{\rm pp} = \int m_{\rm eff}\, ds$ with $ds^2 = g_{ab}dx^a dx^b$ and composition-*independent* $m_{\rm eff}$ in the probe limit. Varying yields the same geodesic equation $\ddot{x}^\mu + \Gamma^\mu_{\alpha\beta}\dot{x}^\alpha\dot{x}^\beta = 0$ for both bodies. Thus the acceleration depends on the *external* field ($\Gamma^\mu_{\alpha\beta}[g]$) but not on the test-body makeup, preserving universality of free fall. *Equivalently: all matter couples minimally to the metric*, ensuring universal geodesic motion and satisfying the Einstein Equivalence Principle within APM's sourcing/response split.

**Mode content and propagation.** The TT branch propagates at $F_q\lambda_C$; the scalar–Aether mode exhibits an achromatic shift $v_g = F_q\lambda_C(1-\epsilon/2)$ with $\epsilon = \pm\alpha$. Interband delay ratios therefore vanish at leading order ($\mathcal{R}_\tau \approx 0$), so observed multimessenger lags are attributed to source physics, consistent with achromatic constraints (Abbott et al., 2017a,b, 2019, 2020).

## 11 Discussion and Outlook

Within the APM ledger $A_u \cdot \mathrm{curl} = {F_q}^2{\lambda_C}^2$, the chronovibrational sector contributes a single scalar–longitudinal polarization with a frequency–even dispersion shift $\epsilon = \pm\alpha$ at leading order, while the TT modes remain on the base cone $\Omega = F_q\lambda_C\, k$. Assigning Aether stretch to curl and sourcing it by neutron content clarifies the mechanism linking massive structure to magnetic rotation and rmfd signatures. The proposed magnetic–first triage, multi–band timing, polarization nulls, and rmfd calibrations comprise a compact experimental program to bound or reveal $\alpha$ and quantify scalar admixture entirely within QMU, while remaining consistent with multimessenger achromatic constraints. (Abbott et al., 2017a,b, 2019, 2020)

## Acknowledgments

We thank collaborators at the Quantum AetherDynamics Institute for continued development of the QMU ledger, and for discussions on chronovibrational calibration with rotating magnetic field resonators.

## References

D. W. Thomson III. APM Chronovibration Notes. preprint (2025).

Quantum AetherDynamics Institute. Aether Physics Model (APM) resources and QMU ledger. `https://sota.aetherwizard.com` (2025).

B. P. Abbott *et al.* (LIGO Scientific Collaboration and Virgo Collaboration). GW170817: Observation of Gravitational Waves from a Binary Neutron Star Inspiral. *Phys. Rev. Lett.* **119**, 161101 (2017). doi:10.1103/PhysRevLett.119.161101.

B. P. Abbott *et al.* (LIGO, Virgo, Fermi GBM, INTEGRAL, ...). Gravitational Waves and Gamma-rays from a Binary Neutron Star Merger: GW170817 and GRB 170817A. *Astrophys. J. Lett.* **848**, L13 (2017). doi:10.3847/2041-8213/aa920c.

T. Callister *et al.* Polarization-Based Tests of Gravity with the Stochastic Gravitational-Wave Background. *Phys. Rev. X* **7**, 041058 (2017). doi:10.1103/PhysRevX.7.041058.

B. P. Abbott *et al.* (LIGO Scientific Collaboration and Virgo Collaboration). Tests of General Relativity with the Binary Black Hole Signals from the LIGO-Virgo Catalog GWTC-1. *Phys. Rev. D* **100**, 104036 (2019). doi:10.1103/PhysRevD.100.104036.

R. Abbott *et al.* (LIGO Scientific Collaboration and Virgo Collaboration). Tests of General Relativity with Binary Black Holes from the LIGO-Virgo Catalog GWTC-2. arXiv:2010.14529 [gr-qc] (2020).

Y. Hagihara, N. Era, D. Iikawa, and H. Asada. Constraining extra gravitational wave polarizations with advanced detectors. *Phys. Rev. D* **100**, 064010 (2019). doi:10.1103/PhysRevD.100.064010.

N. Xie, C. Zhang, Y. Hagihara, N. Era, and H. Asada. Constraining the extra polarization modes of gravitational waves with the GWTC-1 catalog. *Phys. Rev. D* **106**, 124017 (2022). doi:10.1103/PhysRevD.106.124017.

T. Jacobson and D. Mattingly. Einstein-Aether Waves. *Phys. Rev. D* **70**, 024003 (2004). doi:10.1103/PhysRevD.70.024003.

C. Eling, T. Jacobson, and D. Mattingly. Einstein-Aether Theory. arXiv:gr-qc/0410001 (2004).

D. P. Sorokin. Introductory Notes on Non-Linear Electrodynamics and its Applications. arXiv:2112.12118 [hep-th] (2021).

H. F. M. Goenner. On the History of Unified Field Theories. Part II. (ca. 1930–ca. 1965). *Living Rev. Relativity* **17**, 5 (2014). doi:10.12942/lrr-2014-5.

M. J. Neves. Dispersion relations in nonlinear electrodynamics and the Born–Infeld theory. *Phys. Rev. D* **104**, 015006 (2021). doi:10.1103/PhysRevD.104.015006.